

## COMPARATIVE ANALYSIS OF SOLAR AIR CHANNELS, z-SHAPED OBSTACLES ADDED TO IMPROVE FLOW STRUCTURE

by

***Benameur AFIF<sup>a</sup>, Mohamed SALMI<sup>b,c</sup>, Ali AKGUL<sup>d,e,f\*</sup>, Rabab JARRAR<sup>g</sup>,  
Jihad ASAD<sup>g</sup>, and Younes MENNI<sup>h</sup>***

<sup>a</sup>Faculty of Sciences and Technology, University Mustapha Stambouli of Mascara, Algeria

<sup>b</sup>Department of Physics, University of M'sila, M'sila, Algeria

<sup>c</sup>Laboratory of Physics and Chemistry of Materials (LPCM), University of M'sila, M'Sila, Algeria

<sup>d</sup>Department of Computer Science and Mathematics, Lebanese American University, Beirut, Lebanon

<sup>e</sup>Department of Mathematics, Art and Science Faculty, Siirt University, Siirt, Turkey

<sup>f</sup>Mathematics Research Center, Department of Mathematics, Near East University,  
Nicosia/Mersin 10, Turkey

<sup>g</sup>Department of Physics, Faculty of Applied Science, Palestine Technical University- Kadoorie,  
Tulkarm, Palestine

<sup>h</sup>Department of Technology, University Center Salhi Ahmed Naama, (Ctr. Univ. Naama),  
Naama, Algeria

Original scientific paper

<https://doi.org/10.2298/TSCI22S1201A>

*This paper's numerical study, which applies the finite volume approach and SIMPLE algorithm, aims to dynamically analyze airflow through a channel with Z-obstacles. Three distinct models were used to place the Z-barriers inside the channel. According to Demartini et al.'s model (2004) and as depicted in example A from the present analysis, the first Z-barrier (fin) is attached to the top wall (heated) and the second (baffle) to the bottom wall (insulated). The Z-barriers, on the other hand, were positioned in the second model on the same wall (in-line arrangement), either on the top surface (two fins in example B) or on the bottom wall (two baffles in example C). With the help of these studies, fluid dynamics in solar air collectors with barriers will be better understood and designed.*

*Key words: z-barriers, air-flow, turbulent structure, simulation, analysis*

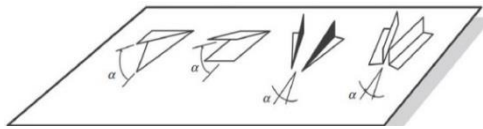
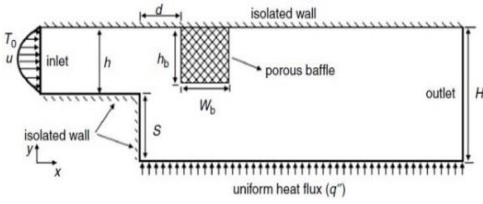
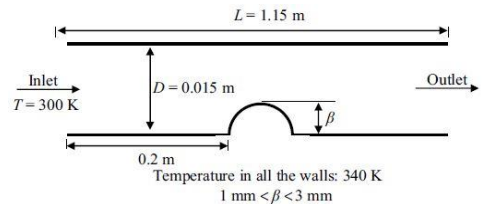
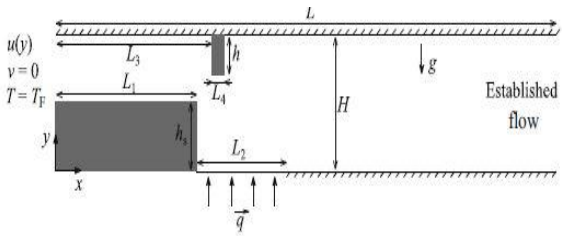
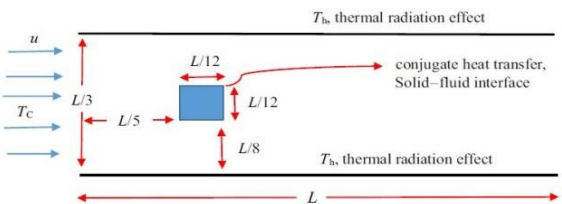
### Introduction

The effectiveness of a solar thermal receiver's channels determines how well it performs overall. One of the most popular techniques when dealing with fluids that have weak physical properties, such as air, water, etc., is channel structure optimization. Access to the use of obstacles, such as baffles, fins and ribs, is one of the best ways to improve the heat structure by enhancing the flow distribution inside the duct [1-5]. Some of the flows in finned, baffled, and/or ribbed channels under various situations are shown in tab. 1. The indicated technique leads to lengthening the flow path, enhancing turbulence, creating strong recirculation regions, and increasing the heat transfer area, which leads to a good improvement in thermal performance [6-10].

---

\*Corresponding author, e-mail: [aliakgul00727@gmail.com](mailto:aliakgul00727@gmail.com)

**Table 1. Fluid-flows around baffled, finned and/or ribbed surfaces**

Author (s)	Physical model	Physical domain
Ahmed <i>et al.</i> [6]	Using vortex generators and nanofluids, heat transport in non-circular ducts is improved	
Li <i>et al.</i> [7]	A porous baffle is used to improve heat transmission and flow analysis in a step that faces backwards	
Zheng <i>et al.</i> [8]	An analysis of the effects of the vortex generator's shape on the turbulent heat transfer of Water/DWCNT-TiO <sub>2</sub> in a channel	
Boudiaf <i>et al.</i> [9]	Numerical analysis of the impacts of viscous dissipation and non-Boussinesq models on the flow of CMC-TiO <sub>2</sub> fluid over a step that faces backward with a baffle	
Peiravi and Alinejad [10]	Simulation of heat transport by convection and radiation in a channel containing a rectangular cylinder	

In this study, three different channel models (A, B, and C) fitted with  $z$ -obstacles are taken into consideration. The heated upper and insulated lower wall-mounted staggered obstacles are taken into account by the first model (A). For the second model (B), hot upper wall-attached in-line fins are proposed and for the third model (C), insulated lower wall-positioned in-line baffles are detailed. The Reynolds number is in the 10000-30000 range. The streamlines, dynamic pressure, mean, axial, and transverse velocities, as well as turbulent kinetic energy, are obtained as contour plots. This work advances the design and understanding of fluid dynamics in solar air collectors with obstacles.

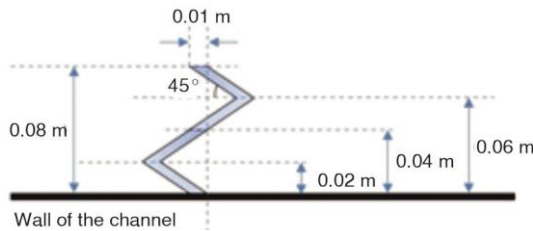


Figure 1. The z-obstacle schematic diagram

### Modelling and simulation

This research investigates air-flows around rectangular z-barriers (obstacles) in a rectangular channel. Figure 1 depicts the schematic diagram of the new obstacle, complete with all of its measurements.

In this investigation, the z-barriers were positioned inside the channel using three different models. According to Demar-

tini *et al.*'s model [11] and as depicted in Case A from the current investigation in fig. 2(a), the first z-barrier (fin) is attached to the top wall (hot) and the second (baffle) to the bottom wall (insulated). The z-barriers were arranged on the same wall (in-line arrangement) in the second model, either on the top surface (two fins in case B) in fig. 2(b) or on the bottom wall (two baffles in case C) as illustrated in fig. 2(c).

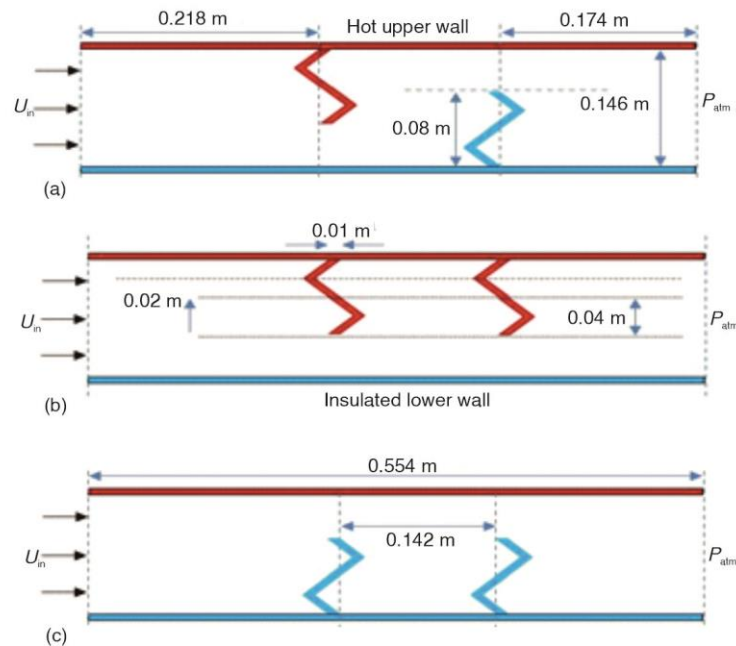


Figure 2. Various situations of the z-obstacles inside the channels;  
 (a) Case (A) – channel with upper and lower z-obstacles,  
 (b) Case (B) – channel with upper z-obstacles, and  
 (c) Case (C) – channel with lower z-obstacles

The following criteria are satisfied in every scenario that is planned:

- A 2-D aspect of an incompressible Newtonian fluid flow (air) with a specified Reynolds number ranging from 10000 to 30000.
- The hydraulic boundary condition at the channel's inlet is a uniform 1-D velocity ( $U_{in}$ ) [11]. At this same section, the temperature of air was set at 300 K.
- The channel's upper wall is subjected to a thermal boundary condition that applied a constant temperature of 375 K [12], with the opposite wall being thermally insulated [13].

– At the channel's exit, the pressure is equal to atmospheric pressure [11].

The continuity, momentum, and energy equations, which govern the simulation of convective air in the specified computational domain, can be expressed using the following common form [14]:

$$\frac{\partial}{\partial x}(\rho u \varphi) + \frac{\partial}{\partial y}(\rho v \varphi) = \frac{\partial}{\partial x} \left[ \Gamma_{\varphi} \frac{\partial \varphi}{\partial x} \right] + \frac{\partial}{\partial y} \left[ \Gamma_{\varphi} \frac{\partial \varphi}{\partial y} \right] + S_{\varphi} \quad (1)$$

where  $u$ ,  $v$ ,  $k$ ,  $\varepsilon$ , and  $T$  are the dependent variables represented by  $\varphi$ ,  $u$  and  $v$  – the velocity components,  $k$  and  $\varepsilon$  – the turbulent kinetic energy and its dissipation ratio, respectively, and  $\Gamma_{\varphi}$  and  $S_{\varphi}$  – the turbulent diffusion coefficient and source term, respectively. The remaining details can be found in Yang and Hwang's numerical analysis [14].

The mesh is non-uniform, and 2-D. All solid limits are where the mesh is refined. For this analysis, the finite volume method, the SIMPLE algorithm, the Second-order upwind and QUICK scheme, the standard  $k$ - $\varepsilon$  model, and the FLUENT software are used to model the convective turbulent air-flow [15-17]. Finally, many of our previous research [2-5] demonstrated the validity of the model by comparing with the data of Demartini *et al.* [11] in the presence of the same geometrical conditions and flow characteristics.

### Findings and discussions

The dynamic pressure,  $P$ , fields' contour plots are displayed in fig. 3. For the lowest Reynolds number values and in each of the cases under study, the  $P$  values are extremely low throughout the whole channel. In the first Case of A,  $P$  values increase as the Reynolds number values increase from 10000 to 30000. This enhancement may be seen on the upper front sharp edge of the  $z$ -fin (first obstacle) and the upper left side of the  $z$ -baffle (second obstacle). On the back of the baffle, close to the hot top surface of the channel, the  $P$  values are extremely high. The  $P$  values are low on the back of both obstacles towards their right sides, on the left side of the fin, and on the lower front side of the baffle. A decrease in dynamic pressure on the entire top part of the channel is brought on in the B second scenario by the presence of impediments (two fins) on the heated upper wall. The gaps between each fin's tip and the insulated bottom surface allow the  $P$  values to increase. Particularly for the highest Reynolds number value, there are excellent  $P$  values close to the lower wall of the channel between the two barriers, however, the  $P$  values are ignored for the smallest Reynolds number value. In the C third instance, which is the opposite of the B second case, the obstacles (two baffles) are fixed to the insulated bottom wall of the channel, with very high  $P$  values on the hot end of the channel near to their upper sides and very low values on their left and right sides.

The streamlines for multiple channel models, including A, B, and C, and various Reynolds number values, including  $Re = 10000$  and  $30000$ , are plotted in fig. 4. A complicated construction with lines that are distorted by the presence of impediments. At the channel's opening, there are parallel and orderly lines. Close to the fin, these lines are distorted. A small cell is created next to the fin's left side as a result of the current being cut off from the channel's heated top wall in the front of this same obstacle. As a result of a decline in pressure levels in this area, this cell is a secondary stream running in the opposite direction. After passing through the front of the fin, the main stream diverges into the first space between the upper face of this fin and the channel's bottom surface. The current splits into two distinct currents after experiencing a second separation on the front top sharp edge of this same fin. Due to low pressure, a very strong cell is generated for recycling in the initial current, which is reversed and is positioned behind the fin. A recycling small cell is formed on the front side of

the baffle by the second current, which is straight and runs towards the left side of this same baffle before diverging at an extremely high speed toward the top section of the channel. The current separates just above the baffle as well, where a very big second cell forms on its right side and extends to the channel's terminus. The current lines are parallel and moving at very high speeds in the upper part of the channel, on the rear side of the baffle. The big recycling cells are definitely behind the obstructions, as is evident. In the figure, it is depicted that for the first Case (A) under study, the intensity and length of recycling cells grow as the Reynolds number values rise.

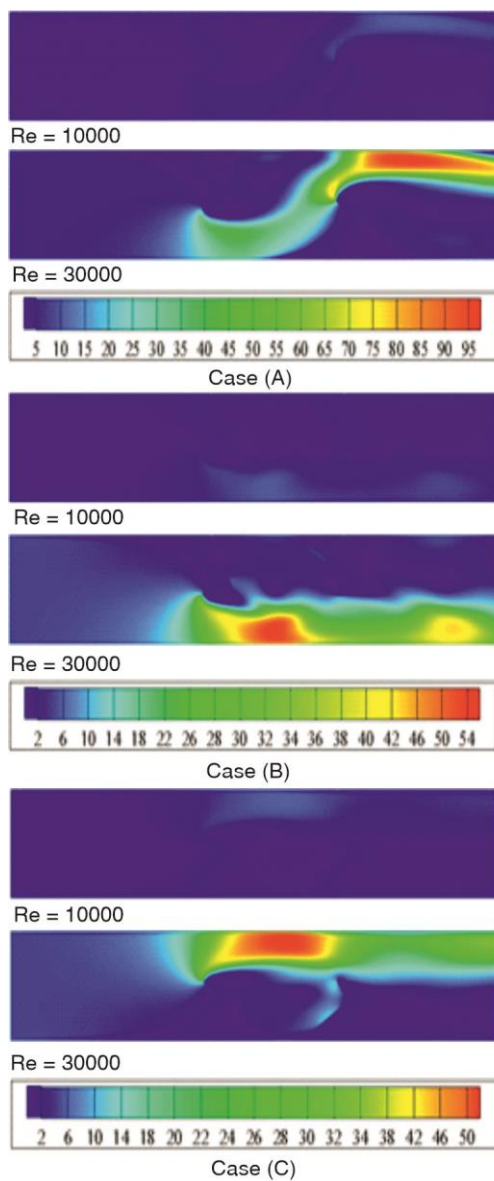


Figure 3. Dynamic pressure fields

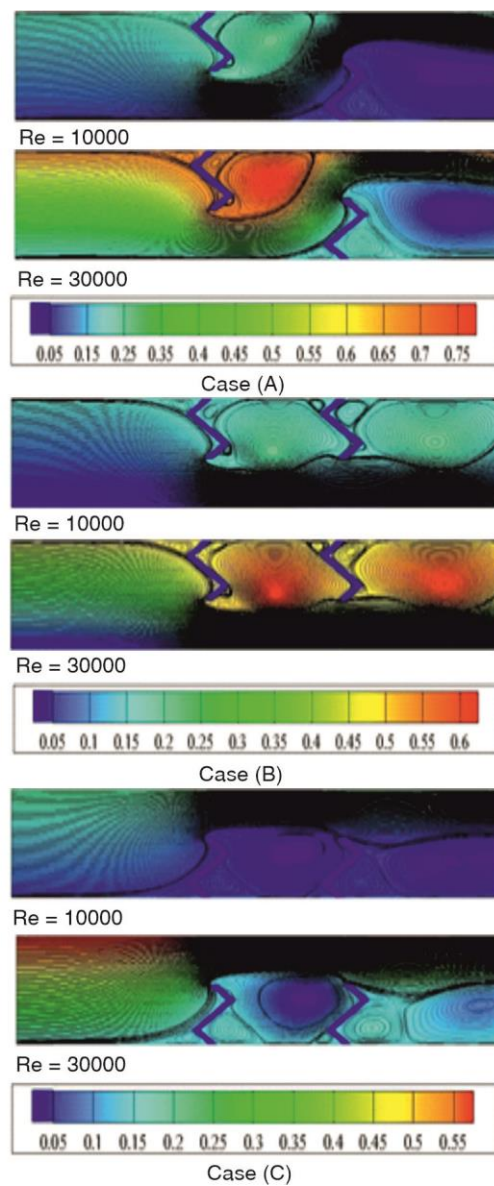


Figure 4. Streamlines

In the case of other models, two extremely powerful recycling cells are situated on the same portion of the channel; in the case of the B second model, on its upper portion, and in the case of the C third model, on its lower portion. Large and cramped between the two obstructions is the first cell. This cell's extension stretches from right side of the first obstacle to the left side of the second obstacle. Two recycling rings make up the second cell. Directly behind the second obstacle is the small first ring. Right next to the first ring, where its extension touches the channel's edge, is the large second ring. Due to the presence of these obstructions between their top face and the opposite channel wall, the current flows through the two gaps in horizontal lines. As predicted, the extension, intensity, strength, and size of recycling cells increase as the Reynolds values increase, enabling the current to flow through the gaps and in each of the two models under consideration at extremely high speeds.

As a result, in each instance, the channel has very powerful rotating cells on the back regions of each obstacle with extremely high velocities across the gaps, where this improvement increases with Reynolds values. Additionally, the A first model with staggered obstacles has very high flow velocities because, in contrast to other models, it has large and sturdy cells that give it a very complex structure.

Figure 5 shows the distribution of mean velocity fields as a function of Reynolds number. The velocity values vary from region to region and according to the applied Reynolds values, as seen in this figure.

The velocity values are decreasing in the first area at the entry. The first obstacle (fin) connecting to the hot top wall is to blame for this decrease in velocity. On the upper left side of the fin, a portion of the fluid circulation has become stagnant. This obstruction causes the current to flow from the top side of the channel to its bottom side through the opening between its sharp edge and the lower, insulated wall. High-speed current travels through this opening in the direction of the second obstacle (baffle) installed on the lower wall. On the left side of the same baffle, the flow's disruption increases. This obstruction accelerates the current to great speeds in the direction of the hot upper region of the channel. From the front sharp edge of the second obstruction to the channel's exit, which is close to the heated top surface, the rise in velocity reaches its greatest value. This behavior is for the A first instance and for Reynolds' great values. The front and rear sides of each obstacles in situations B and C have low velocity values because there is low pressure in these areas. Particularly between obstacles, velocity values are high across gaps. Due to the high pressure values brought on by the existence of these in-line obstructions and the reduction in flow area, particularly for high Reynolds numbers, this acceleration is the result. A very active turbulent structure with extremely high flow velocities results from placing the baffles in accordance with the A first model.

Figure 6 displays the contour plots of axial velocity fields for several channel models, including the A, B, and C cases, and various Reynolds number values, namely  $Re = 10000$  and  $30000$ . Due to the existence of particularly potent recycling cells in these regions, the velocity values are quite low close to the left and right sides of the obstacles, especially on their back surfaces. These cells have negative velocities and are the countercurrents to the main stream. On the sides of the obstacles, current pressure values decreased, which led to the formation of these cells. Due to a reduction in the flow surface and high pressure values, which result in high velocities, there is a first gap between the bottom wall of the channel and the upper sharp edge of the fin. From the second obstacle's front sharp edge until the channel's exit through the hot upper section, the velocity values are very high. The dynamics of air fluid are similarly impacted by changes in Reynolds values. In the back sections of each barrier,

where very large cells are formed for recycling, there is a clear correlation between the rise in Reynolds values and the improvement in flow velocity, and this is true for the A first model under consideration. A sizable zone with extremely high flow velocities spans from the first front sharp edge to the channel exit in the second and third models (B and C), above the first and second obstacles. Near the opposing wall, between the right and left sides of the first and second baffles, respectively, are where the largest velocity values are found. As the Reynolds values rise, so do the speed values. When contrasting these two models, it can be seen that the B second model's construction permits the current to be directed toward the thermally insulated bottom wall, but the C latter model oriented the flow field towards the hot top wall of the channel and so made heat transfer more probable.

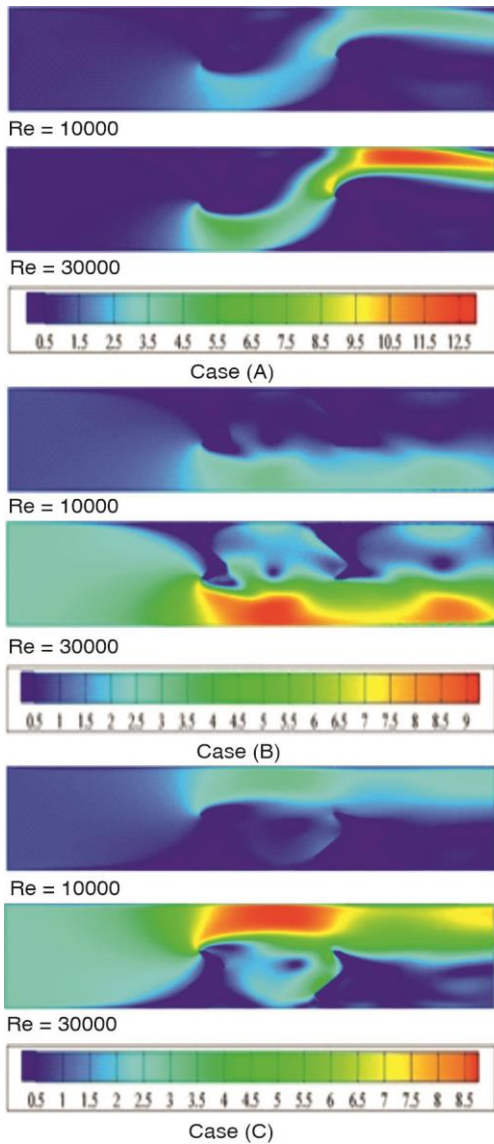


Figure 5. Mean velocity fields

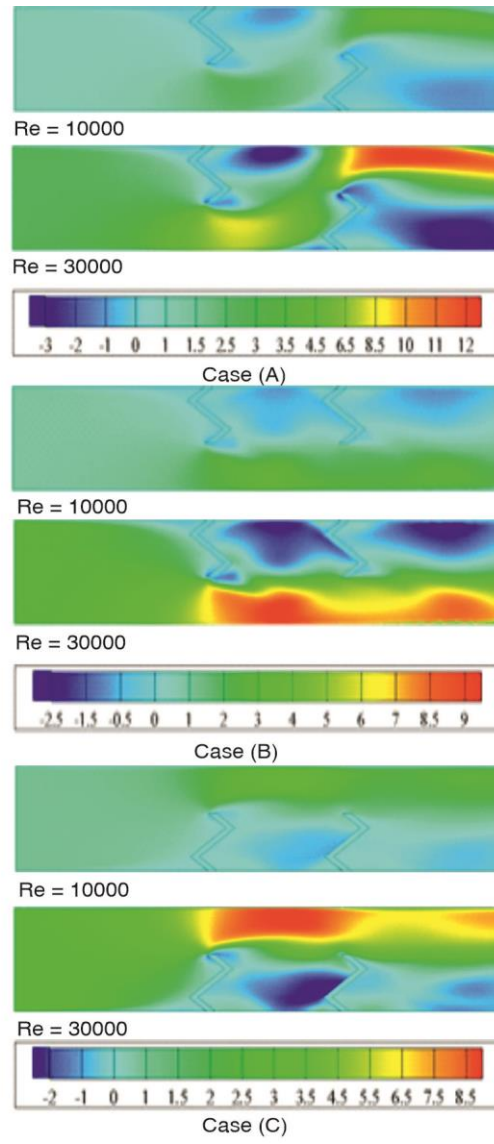


Figure 6. X-velocity fields

The velocity field's transverse component is seen in fig. 7. The A model offers positive large velocities on the front upper sharp edge of the baffle as it directs the current in the direct direction from the bottom of the channel towards its hot upper wall, while there are negative small velocities on the top left side of the fin as a result of changing the passage of the current towards the opposite direction, from the hot part of the channel towards its thermally insulated wall. As expected, the velocity values increased with Reynolds values. The B second model gives the largest velocity values adjacent to the front point of the upper surface of the first fin and the smallest values next to the left side of the second fin. In the C model, the initial barrier on the channel's insulated bottom wall modifies the current's direction by rerouting it at extremely high speeds toward the channel's heated top area, which appears on the front tip of the same obstacle. Due to the existence of reverse flow cells between the two baffles, the negative small velocity values are visible on the front side of the second obstacle. This figure makes it abundantly evident that the first model with staggered obstacles, A, has much higher velocity values than the second and third models, B and C, which have in-line barriers. By forming highly strong and large cells for recycling on the rear areas of both the upper and lower obstacles, this huge improvement in velocity reveals the great deviation of flow from the initial model.

The turbulent kinetic energy,  $k$ , values are very low throughout the various sections of the channels, as illustrated in fig. 8 (case A), and for the least Reynolds number values. With modest Reynolds values, its values are slightly higher. This improvement is seen from the second obstacle's front upper edge to the channel's exit section, which is slightly distant from its hot top wall. In the case of a wide range of Reynolds numbers, a big zone with high kinetic energy forms on the back region of the lower obstacle. The recycling cell area included between the right and front sides of the first and second obstacles, respectively, has somewhat raised  $k$  values in the B second model. Also, for high Reynolds number values,  $k$  values are particularly high close to the channel outlet behind the second obstacle.

The C last model shows the same behavior. It is obvious that the A first model with staggered barriers is the best and optimal design to give the air fluid a strong turbulent structure since, as expected, there is a direct proportion between  $k$  values and Reynolds number values.

## Conclusion

The following are the key conclusions from this research:

- A complicated structure that has lines that are distorted by obstructions. As the Reynolds values increase, the extension, intensity, strength, and size of recycling cells increase, enabling the current to flow through the gaps and in each of the three models under study at extremely high velocities. Compared to other models, the A first model with staggered barriers has highly strong cells and a very complicated structure, which results in a very high flow.
- The A first model with staggered  $z$ -obstacles has very high flow mean velocities because, in comparison to other models, it has large and robust cells and a relatively complicated structure. The  $z$ -obstacles are arranged to provide a very active turbulent structure with extremely high flow  $x$ -velocities according to the A first model.
- It is abundantly obvious from this analysis that the  $y$ -velocity values are significantly higher in the first model with staggered  $z$ -barriers (case A) than in the second and third models with in-line barriers (cases B and C). By forming highly strong and large cells for

recycling on the rear regions of both the upper and lower obstacles, this huge improvement in y-velocity reveals the great departure of flow from the initial model.

- It is evident that the A first model with staggered z-barriers is the best and most ideal configuration to provide the air fluid a robust turbulent structure since, as predicted, there is a direct correlation between turbulent kinetic energy values and Reynolds number values.

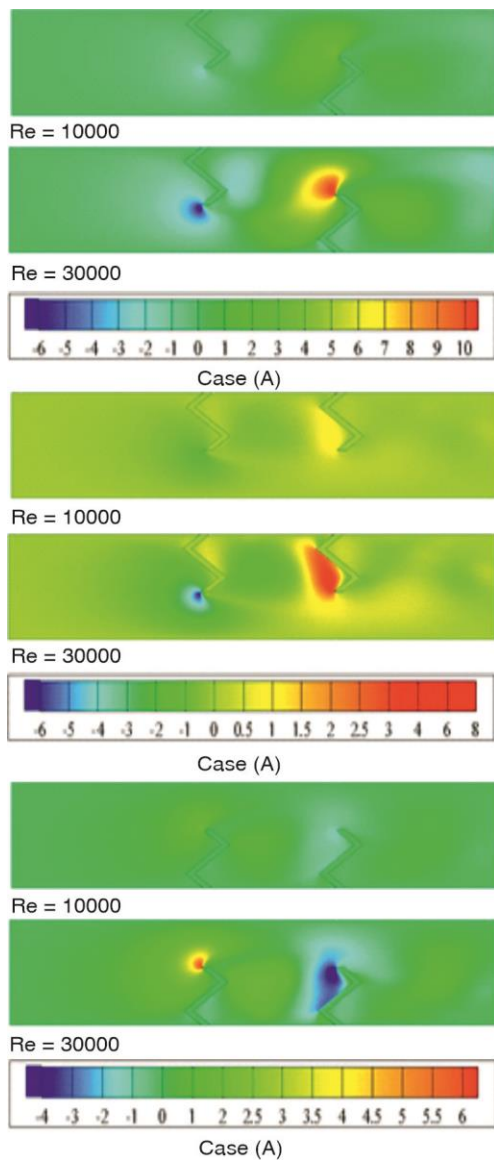


Figure 7. The Y velocity fields

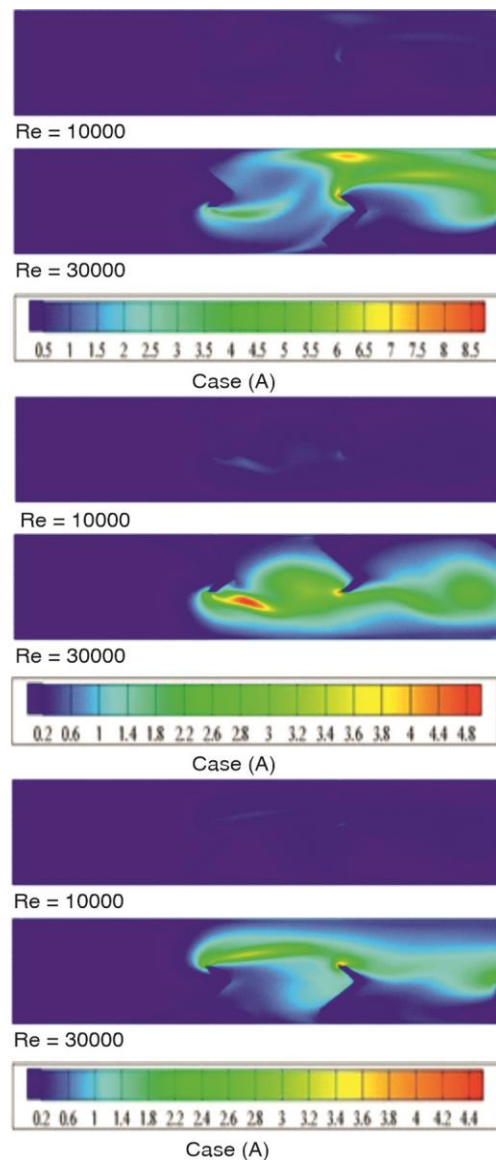


Figure 8. The k energy fields

### Acknowledgment

The authors R. Jarrar and Jihad Asad would like to thank Palestine Technical University- Kadoorie for supporting this work financially.

## References

- [1] Guendouz, N., et al., Study and Analysis of the Dynamic Thermal-Energy Behavior of a Flat Plate Converter System, *Computational Thermal Sciences: An International Journal*, 11 (2019), 3, pp. 233-242
- [2] Menni, Y., et al., Computational Thermal Analysis of Turbulent Forced-Convection Flow in An Air Channel with a Flat Rectangular Fin and Downstream V-Shaped Baffle, *Heat Transfer Research*, 50 (2019), 18, pp. 1781-1818
- [3] Menni, Y., et al., The Solar Air Channels: Comparative Analysis, Introduction of Arc-Shaped Fins to Improve the Thermal Transfer, *Journal of Applied and Computational Mechanics*, 5 (2019), 4, pp. 616-626
- [4] Menni, Y., et al., Numerical Analysis of Fluid Flow and Heat Transfer Characteristics of a New Kind of Vortex Generators by Comparison with Those of Traditional Vortex Generators, *Int. Journal of Fluid Mechanics Research*, 47 (2020), 1, pp. 23-42
- [5] Menni, Y., et al., Use of Waisted Triangular-Shaped Baffles to Enhance Heat Transfer in a Constant Temperature-Surfaced Rectangular Channel, *Journal of Engineering Science and Technology*, 12 (2017), 12, pp. 3251-3273
- [6] Ahmed, H. E., et al. Experimental Study of Heat Transfer Augmentation in Non-Circular Duct Using Combined Nanofluids and Vortex Generator, *Int. Journal of Heat and Mass Transfer*, 90 (2015), Nov., pp. 1197-1206
- [7] Li, C., et al. Enhanced Heat Transfer and Flow Analysis in A Backward-Facing Step Using a Porous Baffle, *Journal of Thermal Analysis and Calorimetry*, 141 (2020), 5, pp. 1919-1932
- [8] Zheng, Y., et al. An Investigation on the Influence of the Shape of the Vortex Generator on Fluid Flow and Turbulent Heat Transfer of Hybrid Nanofluid in a Channel, *Journal of Thermal Analysis and Calorimetry*, 143 (2021), 2, pp. 1425-1438
- [9] Boudiaf, A., et al. Numerical Study of Viscous Dissipation and Non-Boussinesq Model Effects on CMC-TiO<sub>2</sub> Fluid Flow over Backward Facing Step with Baffle, *Journal of Thermal Analysis and Calorimetry*, 135 (2019), 1, pp. 787-799
- [10] Peiravi, M. M., Alinejad, J., Hybrid Conduction, Convection and Radiation Heat Transfer Simulation in a Channel with Rectangular Cylinder, *Journal of Thermal Analysis and Calorimetry*, 140 (2020), 6, pp. 2733-2747
- [11] Demartini, L. C., et al., Numeric and Experimental Analysis of the Turbulent Flow Through a Channel with Baffle Plates, *Journal of the Brazilian Society of Mechanical Sciences and Engineering*, 26 (2004), 2, pp. 153-159
- [12] Nasiruddin, M. H., Siddiqui, K., Heat Transfer Augmentation in a Heat Exchanger Tube Using a Baffle, *Int. Journal of Heat and Fluid Flow*, 28 (2007), 2, pp. 318-328
- [13] Dutta, P., Hossain, A., Internal Cooling Augmentation in Rectangular Channel Using Two Inclined Baffles, *Int. Journal of Heat and Fluid Flow*, 26 (2005), 2, pp. 223-232
- [14] Yang, Y. T., Hwang, C. Z., Calculation of Turbulent Flow and Heat Transfer in a Porous-Baffled Channel, *Int. Journal of Heat and Mass Transfer*, 46 (2003), 5, pp. 771-780
- [15] Patankar, S. V., *Numerical Heat Transfer and Fluid Flow*, McGraw-Hill, New York, USA, 1980
- [16] Leonard, B. P., Mokhtari, S., Ultra-Sharp Non-Oscillatory Convection Schemes for High-Speed Steady Multidimensional Flow, NASA TM 1-2568, NASA Lewis Research Center, Cleveland, O., USA, 1990
- [17] Launder, B. E., Spalding, D. B., The Numerical Computation of Turbulent Flow, *Computer Methods in Applied Mechanics and Engineering*, 3 (1974), 2, pp. 269-289